Phase transitions in Schloegl's second model for autocatalysis on a Bethe lattice

Da-Jiang Liu,[1] Chi-Jen Wang,[2] and James W. Evans[1,3]
[1]*Ames Laboratory—USDOE, Iowa State University, Ames, Iowa 50011, USA*
[2]*Department of Mathematics, National Chung Cheng University, Chiayi 62102, Taiwan*
[3]*Department of Physics & Astronomy and Department of Mathematics, Iowa State University, Ames, Iowa 50011, USA*

(Received 12 February 2021; revised 16 April 2021; accepted 24 June 2021; published 26 July 2021)

Schloegl's second model (also known as the quadratic contact process) on a lattice involves spontaneous particle annihilation at rate p and autocatalytic particle creation at empty sites with $n \geqslant 2$ occupied neighbors. The particle creation rate for exactly n occupied neighbors is selected here as $n(n-1)/[z(z-1)]$ for lattice coordination number z. We analyze this model on a Bethe lattice. Precise behavior for stochastic models on regular periodic infinite lattices is usually surmised from kinetic Monte Carlo simulation on a finite lattice with periodic boundary conditions. However, the persistence of boundary effects for a Bethe lattice complicates this process, e.g., by inducing spatially heterogenous states. This motivates the exploration of various boundary conditions and unconventional simulation ensembles on the Bethe lattice to predict behavior for infinite size. We focus on $z = 3$, and predict a discontinuous transition to the vacuum state on the infinite lattice when p exceeds a threshold value of around 0.053.

DOI: 10.1103/PhysRevE.104.014135

I. INTRODUCTION

There remain fundamental challenges in understanding nonequilibrium phase transitions in stochastic lattice-gas models where the rates for processes defining the model do not satisfy a detailed-balance condition [1–3]. Perhaps the optimal prototype for analysis of discontinuous nonequilibrium phase transitions is Schloegl's second model [4] involving spontaneous particle annihilation at rate p, and autocatalytic particle creation at empty sites with two or more occupied neighbors [5,6]. This model is equivalent to the quadratic contact process on a lattice where infected sites spontaneously recover, and healthy sites can be infected if they have two or more sick neighbors [5]. Different prescriptions are possible for the particle creation rates, e.g., a "threshold" choice with a single creation rate of $r = 1$ for all configurations with $n \geqslant 2$ occupied neighbors [7,8], or a "combinatorial" choice of creation rate

$$r_n = \binom{n}{2} \Big/ \binom{z}{2} = \frac{n(n-1)}{z(z-1)} \tag{1}$$

for empty sites with n occupied neighbors (out of a total of z neighbors) [9]. Here, z corresponds to the lattice coordination number. The latter choice has some advantages allowing simplification of the exact master equations [9]. However, qualitative behavior of the model does not seem to depend on the specific choice of creation rates.

Since an exact solution of the corresponding master equations is not possible, precise assessment of model behavior on conventional (Euclidean) periodic lattices in the limit of infinite size is usually surmised from kinetic Monte Carlo (KMC) simulation on finite lattices with periodic boundary conditions (BCs). Such analysis for various versions of Schloegl's second model on a square lattice reveals the presence of a discontinuous phase transition to the trivial absorbing vacuum state (with no particles) for sufficiently high p [6,8,9]. There are also some subtleties such as the existence of generic two-phase coexistence which are described elsewhere and not discussed further here [6,8,9].

Bethe lattices [10], finite versions of which correspond to regular Cayley trees [11], have played a significant role in statistical mechanics. Sometimes exact solution of interacting particle systems or percolation problems on Bethe lattices is possible being facilitated by the lack of closed loops or cycles on the lattice [11–15]. Bethe lattices also constitute a special case of more general networks for which there is extensive interest in analysis of cooperative phenomena [15]. Thus, it is natural to consider the behavior of Schloegl's second model on Bethe lattices, our focus here. We will consider primarily the case of coordination number $z = 3$. Indeed, there have been previous analyses in the mathematical statistics literature for discrete and continuous time threshold versions of the model [16,17], as well as an analysis on more complex random graph type networks [18].

However, a significant complication for the use of KMC analysis on finite Bethe lattices to extract behavior for infinite lattice is the persistence of boundary effects [15,19,20]. We address this issue by exploring various BCs in an attempt to identify the optimal choices which minimize finite size effects. We also exploit unconventional simulation ensembles which aid assessment of behavior for an infinite system.

Site labeling for the Bethe lattice used for Schloegl model analysis is described in Sec. II. The hierarchical version of the exact master equations for the Schloegl model which describe heterogeneous (as well as homogeneous) states, and truncation approximations to these equations, are described in

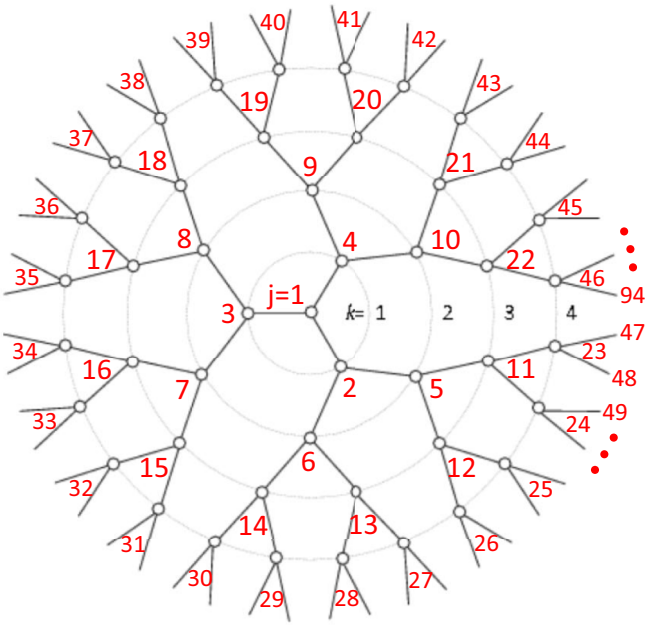

FIG. 1. Schematic of Bethe lattice for $z = 3$. Rings (or shells) are labeled $k = 1, 2, \ldots$ Site labels are in red.

Sec. III. So-called constant-coverage (CC) KMC simulations of steady-state behavior in the model are described in Sec. IV. Refined versions of these CC simulations, as well as conventional continuous time constant-p simulations of time evolution, are presented in Sec. V. Some insights from an analytic treatment are presented in Sec. VI. Conclusions are provided in Sec. VII.

II. BETHE LATTICE SITE LABELING FOR SCHLOEGL MODEL ANALYSIS

We represent either finite or infinite Bethe lattices as having a central site R_0 labeled $j = 1$; R_0 is surrounded by a ring or shell R_1 of z sites labeled $j = 2, 3, \ldots, z+1$; R_1 is surrounded by second ring R_2 with a total of $z(z-1)$ sites labeled $j = z+2, \ldots, 1+z^2$ such that each site in R_1 is connected to $z-1$ sites in R_2; etc. More generally, the kth ring, R_k, has $z(z-1)^{k-1}$ sites, where the site labels j satisfy

$$[z(z-1)^{k-1} - 2]/(z-2) < j \leqslant [z(z-1)^k - 2]/(z-2) \quad \text{for ring } R_k. \tag{2}$$

With this labeling system, it is straightforward to identify the z neighbors of any site, a requirement for developing a KMC simulation algorithm. See the Supplemental Material (SM) [21]. Figure 1 illustrates the above geometry and site labeling for $z = 3$.

We consider the combinatorial version of Schloegl's second model described in Sec. I on such Bethe lattices. Our ultimate goal is to characterize behavior on an infinite Bethe lattice. However, our simulation analysis is performed on a finite Bethe lattice (or Cayley tree) where particles are annihilated and created on the first k^* rings R_k for $1 \leqslant k \leqslant k^*$ subject to boundary conditions (BCs) imposed on ring R_{k^*+1}. The BCs are described in detail in Sec. IV. Note that for large k^*, the number of boundary sites, B_{k^*+1}, in ring R_{k^*+1} and the total number of sites N_{k^*} in rings R_1 through R_{k^*} are given by

$$B_{k^*+1} = z(z-1)^{k^*} \quad \text{and} \quad N_{k^*} = [z(z-1)^{k^*} - 2]/(z-2) \sim z(z-2)^{-1}(z-1)^{k^*}. \tag{3}$$

These quantities are comparable for $z = 3$, and B_{k^*+1} actually exceeds N_{k^*} for $z > 3$.

III. HETEROGENEOUS HIERARCHICAL MASTER EQUATIONS

An exact analytic formulation of behavior of the stochastic model on finite or infinite lattices can be based on the appropriate master equations. We present the hierarchical version of these equations [22,23] where the evolution equation for the probability that a specific site is occupied couples to probabilities for ensembles of multiple sites with various configurations. Evolution equations for those multisite ensemble probabilities couple to probabilities for even larger ensembles. Analysis of this hierarchy of equations generally requires the application of some type of hierarchical truncation approximation, where probabilities of larger ensembles or sites are written in terms of probabilities for smaller ensembles [1,24,25].

In presenting these equations, we also allow for the possibility of spatially heterogeneous states [22,23], but only states with "circular symmetry" wherein all sites in a given ring are equivalent. Such states will occur on a finite lattice for choices of boundary conditions incorporating this symmetry, as applies for all our choices. The probability, $P\bullet_k$, for a site in ring k to be occupied (•), i.e., the particle "concentration" in ring k, satisfies

$$d/dt P\bullet_k = -pP\bullet_k (\text{spontaneous annihilation}) + \text{gain terms (autocatalytic creation)}. \tag{4}$$

The gain terms account for all possible $\binom{z}{n}$ configurations of the z neighboring sites of an empty (o) site in ring k with n populated sites and $z-n$ empty sites, where the number n of populated sites ranges over $2 \leqslant n \leqslant z$. The overall gain term involves a sum over the probability of these configurations times the appropriate creation rates r_n. Thus, this "primitive" form of the master equations is somewhat unwieldy involving a sum over a large number of particle creation terms for $2 \leqslant n \leqslant z$ occupied sites neighboring the empty site. However, due to our special combinatorial choice of rates, r_n, these gain terms can be simplified or exactly reduced to involve a sum over probabilities of just triples of sites where the site in ring k is empty, and one considers all possible pairs of occupied neighbors of that site. This exact reduction uses conservation of probability relations, and is described in detail for the combinatorial version of Schloegl's second model in Ref. [9]. As an aside, we note that an analogous exact reduction of particle creation terms is also possible in the master equations for Durrett's version of Schloegl's second model, as described in detail in Refs. [22,23]. Then, accounting for the equal probabilities of many of these configurations, (4) adopts the form shown in Fig. 2(a). Separate treatment is naturally

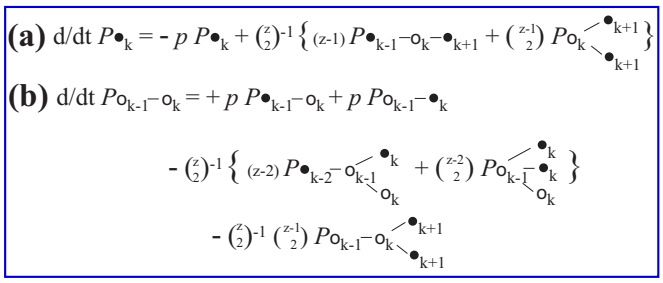

FIG. 2. Low-order hierarchical master equations for heterogeneous states. (a) Evolution equation for the probability of an occupied site, $P\bullet_k$, in ring $k \geqslant 1$. (b) Evolution equation, $Po_{k-1}o_k$ for the probability of a neighboring empty pair of sites, one in ring $k-1$ and the other in ring k. Note that the second loss term with the factor $\binom{z-2}{2}$ is absent for $z = 3$. Notation: $P\bullet_{k-1} - o_k$ (or more concisely $P\bullet_{k-1}o_k$) denotes the probability of a neighboring filled site in ring $k-1$ and an empty site in ring k; $P\bullet_{k-1} - o_k - \bullet_{k+1}$ (or $P\bullet_{k-1}o_k\bullet_{k+1}$) denotes the probability a triple of sites with a filled site in ring k, an empty site in ring $k-1$, and an empty site in ring $k+1$, where sites in adjacent rings are neighbors; etc. Thin lines are included in the figure to indicate bonds between neighboring sites and thus indicate lattice structure. Note that $\binom{z}{2}^{-1} = k_2$ is the rate for particle creation at an empty site with exactly two occupied neighbors.

needed for site $j = 1$ in R_0, and also for the outer boundary sites for a finite lattice.

The simplest mean-field (MF) or site approximation factorizes multisite probabilities as a product of single-site probabilities. Introducing the notation $C_k = P\bullet_k$ for the concentration of particles in ring k, then in the MF approximation one has for example that

$$P\bullet_{k-1}o_k\bullet_{k+1} \approx C_{k-1}(1 - C_k)C_{k+1}. \tag{5}$$

Then, the MF version of the equations in Fig. 2(a) become a set of lattice differential equations (also known as discrete reaction-diffusion equations or dRDEs),

$$d/dtC_k = -pC_k + (1 - C_k)C_{k+1}[2C_{k-1} + (z - 2)C_{k+1}]/z, \quad \text{for } k \geqslant 1, \tag{6}$$

supplemented by

$$d/dtC_0 = -pC_0 + (1 - C_0)(C_1)^2, \quad \text{for } k = 0. \tag{7}$$

In a MF analysis of the special case of a spatially homogenous state (i.e., a state which is spatially uniform in an ensemble or statistically averaged sense) where $C_k = C$ independent of k, (6) and (7) reduce to the familiar MF kinetics for Schloegl's second model where [4,23]

$$d/dtC = -pC + (1 - C)C^2 \text{ independent of } z, \tag{8}$$

with corresponding steady states [4,23],

$$C_\pm(\text{site}) = \frac{1}{2} \pm \frac{1}{2}(1 - 4p)^{1/2} \quad \text{for} \quad 0 \leqslant p \leqslant p_s(\text{site}) = \frac{1}{4}, \quad \text{and } C_{\text{vac}} = 0. \tag{9}$$

Here C_+ and C_{vac} are stable, and C_- is an unstable steady state. $C_\pm$ are populated states, and C_{vac} is the trivial absorbing vacuum state. C_+ and C_- disappear beyond the spinodal point p_s, a sn bifurcation. We caution, however, that MF site approximation predictions provide a poor description of exact model behavior [9].

Despite their neglect in the MF treatment, there do exist significant spatial correlations in the model. More specifically, autocatalytic particle creation naturally induces clustering of particles on the lattice, and consequently also clustering of empty sites. Thus, a more effective higher-level hierarchical truncation approximation is provided by the *pair approximation* [8,22,23] which attempts to incorporate these correlations. One starts with the evolution equations for $P\bullet_k = C_k$ and for the probability of an adjacent empty pair of sites, $Po_{k-1}o_k = D_{k-1,k}$, say, as shown in Figs. 2(a) and 2(b), respectively. One then factorizes probabilities of triplets and larger ensembles of sites as a product of constituent pair probabilities, also compensating for overcounting of sites. Thus, for example, one obtains

$$P\bullet_{k-1}o_k\bullet_{k+1} \approx P\bullet_{k-1}o_kPo_k\bullet_{k+1}/Po_k, \tag{10}$$

where the right-hand side can be written in terms of C_k, $D_{k-1,k}$, and $D_{k,k+1}$ utilizing conservation of probability relations. Applying this procedure to the equations indicated in Fig. 2 generates a closed coupled set of lattice differential equations for the C_k and for $D_{k-1,k}$. See Appendix A for details.

As an aside, we note that rather than pair probabilities, $Po_{k-1}o_k$, $P\bullet_{k-1}o_k$, etc., for some analyses it is natural to introduce as alternative variables the conditional probabilities or concentrations, $K_{k|k-1} = Po_{k-1} - \bullet_k/Po_{k-1}$ or $K_{k|k+1} = P\bullet_k - o_{k+1}/Po_{k+1}$ for finding an occupied site in ring k given an adjacent empty site in ring $k-1$ or ring $k+1$, respectively.

In a pair approximation analysis of the special case of a spatially homogenous state or a "spatially uniform" state, not just $C = C_k$ is independent of k, but all pair, triplet, etc., probabilities are also independent of location in the system. A consequence of the latter is that there is a unique conditional concentration

$$K = K_{k|k-1} = K_{k|k+1} = P \bullet o/Po \tag{11}$$

of finding an occupied site adjacent to a specified empty site (which is independent of k). Indeed, K is a natural variable for our analysis, as will be clear from the following. The pair approximation [23] for homogeneous states yields

$$d/dtC = -pC + (1 - C)K^2 \quad \text{and} \quad d/dt\, Poo = 2P \bullet o[p - (z - 2)K(1 - K)/z]. \tag{12}$$

Analysis of steady state behavior finds a stable populated steady state with

$$K_\pm(\text{pair}) = \frac{1}{2} \pm \frac{1}{2}[1 - 4zp/(z - 2)]^{1/2} \tag{13}$$

and

$$\begin{aligned} C_\pm(\text{pair}) &= (K_\pm)^2/[p + (K_\pm)^2] \\ &= 1/\{1 + 1/[K_\pm/p - z/(z-2)]\} \\ &= 1 - \frac{1}{2}\{-1 + 4p/(z - 2) \pm [1 - 4zp/(z - 2)]^{1/2}\}/ \\ &\quad [1 + 4p/(z - 2)^2], \end{aligned} \tag{14}$$

for $0 \leqslant p \leqslant p_s(\text{pair}) = (z-2)/(4z)$, the spinodal point. Again, C_+ and C_- correspond to stable and unstable populated steady states, respectively, as do K_+ and K_-. There also exists a vacuum steady state $C_{\text{vac}}(\text{pair}) = K_{\text{vac}}(\text{pair}) = 0$. For our subsequent analysis, it is also instructive to note that the conditional probability or concentration in the pair approximation satisfies both

$$K = (z-2)C/(z-2C) \quad \text{and} \quad K = [pC/(1-C)]^{1/2}, \tag{15}$$

for the stable and unstable populated states. The above-mentioned clustering of particles implies anticlustering of filled-empty pairs which means that $K < C$, consistent with the first relation in (15). We note that the same pair approximation results apply for a hypercubic lattice with (even) coordination number z [23]. Also, as expected in this spatially homogenous case, the pair approximation recovers MF behavior in the limit as $z \to \infty$.

Higher-order truncation approximations are also possible including the triplet approximation which retains probabilities of adjacent triples of sites (as well as probabilities of pairs and single sites), the quartet approximation which retains probabilities of adjacent quartets of sites, etc. However, while there is generally a substantial improvement in predictive capability going from the site to the pair approximation, only relatively minor improvements are seen for higher-order approximations. Thus, we do not discuss the latter further in this study.

IV. CC-ENSEMBLE SIMULATION ANALYSIS FOR FINITE $z = 3$ BETHE LATTICES

KMC simulations for our combinatorial version of Schloegl's second model are performed on finite Bethe lattices where particles are created and annihilate on rings R_1 through R_{k^*}, and boundary conditions (BCs) are imposed at ring R_{k^*+1}. Conventional (constant p) simulation of evolution in this continuous-time Markovian model implements particle creation and annihilation processes with probabilities proportional to their rates. Since there is not a significant spread in rates for the model, we do not use a rejection-free algorithm but rather a basic algorithm. In this case, sites are selected at random and events implemented with probabilities proportional to the relevant rates for a specified particle annihilation rate, p. For analysis of time evolution of the model in Sec. V, we perform such simulation tracking time in terms of the number of Monte Carlo steps per site (with a suitable normalization based upon the maximum rate). When such simulations are run for sufficient time to reach a stable steady state, and where this process is repeated for a number of different p values, one can extract the variation of the steady-state $C = C(p)$ for such states.

Indeed, most of our analysis focuses on characterization of steady-state behavior. However, it is convenient and efficient to utilize instead a constant-coverage (CC) simulation ensemble, or some modification thereof. In a standard CC ensemble simulation [26], a target concentration $C = C_t$ for the entire system is selected, and particle annihilation (creation) is attempted if the actual concentration is above (below) the target. When particle creation is attempted, it occurs with probabilities reflecting the prescribed rates, r_n, in our combinatorial version of Schloegl's second model. From the fraction of attempts at annihilation, one extracts the p value corresponding to the target value $C = C_t$. Thus, running such simulations for a number of different target C_t, one can extract $p = p(C)$ for the steady state. This functional relationship can be inverted to obtain $C = C(p)$. For an infinite system, the constant-p and CC simulation ensemble produce identical results analogous to canonical versus grand canonical simulation of equilibrium systems. This equivalence of ensembles for nonequilibrium models is discussed and confirmed in Ref. [27] for standard Euclidean lattices, but previous analysis for Bethe lattices is lacking. For finite systems, some differences arise, as discussed below.

We consider five choices of BCs as a way to provide additional insight, and to better assess behavior in the limit of an infinite lattice. All these choices utilize information on particle concentration and spatial correlations obtained on-the-fly from the CC simulation itself. An extreme active choice of BCs [BC_{act}], which assigns all sites of ring R_{k^*+1} to be permanently occupied, most strongly "enhances" populated states. This BC clearly precludes a transition to the vacuum state. A different mean-field type choice of BCs [BC_{MF}] randomly assigns sites in ring R_{k^*+1} to be occupied with probability $\langle C \rangle$, where $\langle C \rangle$ is the mean population of sites in rings R_1 through R_{k^*}. The MF choice neglects all spatial correlations, which are significant in the model. Thus, we also consider a set of refined "correlated" choices of BCs [BC_{Pa}, BC_{Pb}, BC_{Pc}], described below, which attempts to account for spatial correlations estimated at the level of the pair (P) approximation in determining the occupancy of sites in ring R_{k^*+1}.

Noting that the state of sites in ring R_{k^*+1} is only relevant when attempting to create a particle at an empty site in ring R_{k^*}, correlated choices of BCs randomly assign sites in ring R_{k^*+1} to be populated with probability $K = P \bullet o/Po$ using some estimate of this conditional probability. Two of these choices estimate K from either

$$\begin{aligned} K = K_a &= \langle C \rangle/(3 - 2\langle C \rangle)\ [\text{BC}_{\text{Pa}}], \\ \text{or} \quad K = K_b &= [p\langle C \rangle/(1 - \langle C \rangle)]^{1/2}\ [\text{BC}_{\text{Pb}}], \end{aligned} \tag{16}$$

motivated by the pair approximation relations (15). Plausibly, BC_{Pb} is more effective than BC_{Pa} as it incorporates an estimate of $K = K_b$ which is based upon the exact steady-state relation, $pC = (1-C)Q$, where Q is the conditional probability of a pair of occupied sites adjacent to a specified empty site [cf. Fig. 2(a)]. Thus, the only approximation in determining K_b is the assumption that $Q = K^2$. We anticipate that a treatment [BC_{Pc}] superior to either BC_{Pa} or BC_{Pb} comes from determining the conditional probability, $K = K_c$, exactly from simulated configurations.

Next, we present KMC simulation results for model behavior when $z = 3$ with different BCs, thereby revealing a strong dependence on BCs. As an aside, we note that the "best" choice of BC should be the one where behavior in the finite system most closely mimics that of an infinite system. In this respect, we anticipate that BC_{act} is the worst, and BC_{Pc} is the best BC. Figure 3 shows the results from CC simulations for the steady-state C versus p on a Bethe lattice with $k^* = 16$ rings (i.e., BC are imposed on R_{17}) for the various BCs. Also shown are the site and pair approximation predictions for an

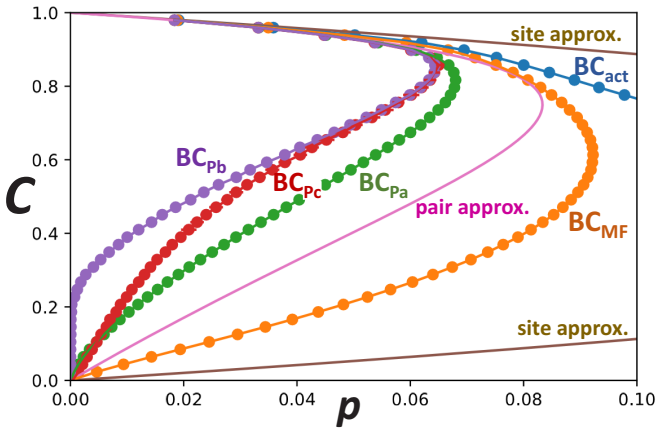

FIG. 3. CC-ensemble KMC simulation results for the global steady-state concentration C versus p for Schloegl's second model on a finite Bethe lattice with $z = 3$ and BC at R_{17}. Each data point is obtained as an average over 10^4 Monte Carlo steps (MCSs). Also shown are results for the site and pair approximation for an infinite homogeneous system corresponding to Eqs. (9) and (14), respectively.

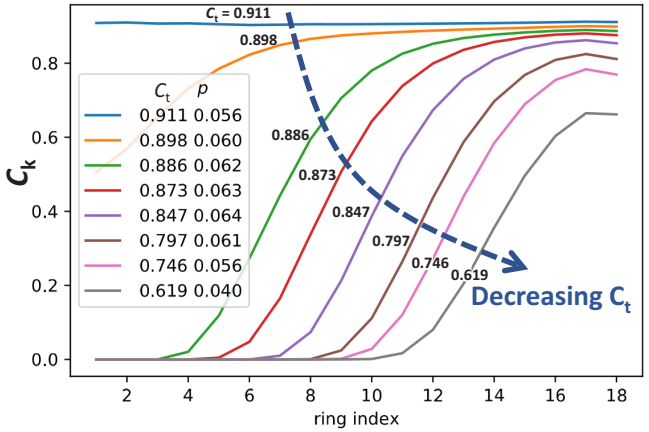

FIG. 4. CC-ensemble KMC simulation results for ring concentrations C_k versus ring index k for Schloegl's second model on a finite Bethe lattice with $z = 3$ and BC_{Pc} imposed at R_{18}.

infinite system corresponding to (9) and (14), respectively. A prominent feature of all approximations, except BC_{act}, is an apparent regime of bistability for some $0 \leqslant p \leqslant p_s$ with coexisting stable high-concentration populated and vacuum states, in addition to a steady state with intermediate concentration. Traditionally, the intermediate concentration state would be identified as unstable, noting that the CC ensemble has the advantage of automatically probing stable as well as unstable steady states [28,29]. Such bistability is in contrast to a discontinuous transition (with associated metastability and hysteresis) anticipated for the model on an infinite Bethe lattice. (Such discontinuous transitions are also realized for infinite regular Euclidean lattices.)

The extent of the bistable loops in Fig. 3 is substantial, and the intermediate concentration steady state seems robust in CC simulations. These features are reminiscent of those seen in analytic mean-field type treatments, and also in CC simulations of so-called hybrid stochastic lattice-gas models, where for the monomer-dimer reaction, the monomer concentration is treated as a global variable due to high monomer mobility, but dimers are treated explicitly in the lattice-gas modeling [28–32]. The origin of the strong bistability in such hybrid models lies in the feature that the critical radius of a droplet of the more stable phase embedded in the less stable phase scales like the diffusion length [29,33–35]. Thus, the critical droplet has a macroscopic size for high mobility, thereby inducing bistability (or more precisely very long-lived mestastability). A spatially uniform unstable steady state is stabilized in CC simulations, whereas for conventional constant p simulations on a finite lattice, the system makes transitions between the two stable steady states [30–32].

The presence of a global monomer concentration in the hybrid monomer-dimer reaction model is reminiscent of our use of a BC for the Schloegl model on the Bethe lattice with C or K determined as a global average. This type of BC could facilitate the strong bistability observed in our CC simulations for a Bethe lattice. However, more detailed analysis reveals distinct behavior between the hybrid monomer-dimer model on a Euclidean lattice with a homogeneous unstable steady-state hybrid and the Schloegl model on the finite Bethe lattice which has a heterogeneous unstable steady state. Figure 4 shows the variation of ring concentration with ring label k for different target concentrations C_t in our simulations of Schloegl's second model with boundary condition BC_{Pc}. For all $C_t < 0.9$ corresponding to the unstable state, there is a strong decrease in ring concentration approaching the central ring R_0 or site $k = 0$.

For the active boundary condition BC_{act}, there is no bistability, and instead a unique stable populated steady state persists for all p. For large p, it is clear that the dominant contribution to the particle population (not including the specified populated boundary sites) will come from ring R_{k^*} where there is a rough balance between the rate of creation of particles, $R_{create} = r_2(1 - C_{k^*}) = (1 - C_{k^*})/3$ induced by the two populated sites in ring $k^* + 1$, noting that the neighboring site in ring $k^* - 1$ is typically empty, and the rate of spontaneous annihilation $R_{annih} = pC_{k^*}$, so that

$$C_{k^*} \approx 1/(1 + 3p), \quad \text{for large } p. \tag{17}$$

Then, using $C_k \approx 0$ for $k < k^*$, and accounting for the number of sites in various rings, implies that the mean concentration for the entire system satisfies

$$C \approx 3 \times 2^{k^*-1}[3 \times 2^{k^*} - 2]^{-1} C_{k^*} \approx 1/(2 + 6p) \quad \text{for large } k (\text{and } p). \tag{18}$$

Figure 3 just captures the onset of this decrease in C with increasing p for BC_{act}.

As noted above, the model does display significant spatial correlations. These are quantified in Fig. 5 comparing simulation results for the exact $K = K_c$ and for K_b versus C with the analytic estimate K_a versus C. Thus, we anticipate that behavior for correlated BCs, BC_{Pa-c}, gives the best indication of stochastic model behavior for an infinite Bethe lattice. One caveat is that we expect bistability will be replaced in the stochastic model by a discontinuous transition occurring somewhat below the spinodal points for these approximations

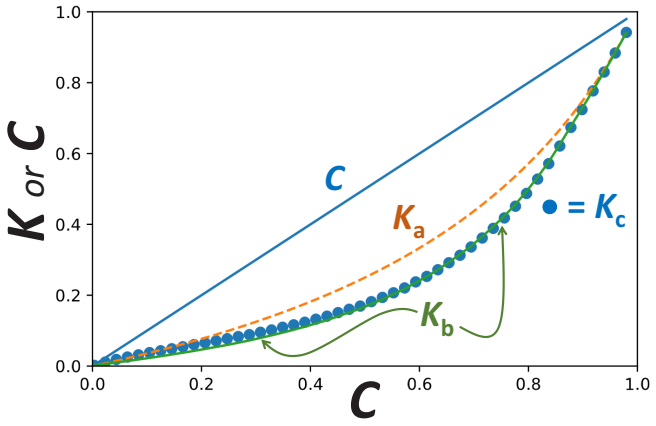

FIG. 5. KMC simulation results for the conditional concentrations, $K = K_c$ and K_b versus C, compared with the analytic prediction, K_a versus C, from the pair approximation.

which are in the range $p_s \approx 0.063$–0.068. This scenario is realized in Schloegl's second model on Euclidean lattices where the location of the transition is determined in analytic approximations by a kinetic analog of a Maxwell construction [8,22,29].

V. SIMULATIONS USING OTHER ENSEMBLES FOR FINITE $z = 3$ BETHE LATTICES

Further insight into model behavior for an infinite system comes from the expectation that the BC will most strongly impact behavior in the outer rings of a finite system, but less so for the more central rings. Here, we are exploiting the observation that the steady states generated in the CC ensemble can be heterogeneous. This observation motivates development and implementation of modified CC simulation algorithms where the concentration which is compared with the target value is just obtained by sampling a specific ring or subset of central rings in the system (rather than sampling the entire system). Figure 6 shows the results of implementing this procedure where a specific ring R_k with $k = k_{CC}$ is sampled. Behavior is compared for BC_{MF} and BC_{Pc}. Similar results are obtained if instead of sampling a single ring with $k = k_{CC}$, a subset of rings Rj with $j = 1$ to k_{CC} are sampled. See Appendix B. Despite the very different behavior for these BCs using the standard CC algorithm, more similar features emerge when selecting $k_{CC} = 8-10$ for $k^* = 16$, i.e., when just sampling the central rings. Resulting behavior is less impacted by special BC-induced behavior at outer rings near the boundary. Using inner rings for small k_{CC} seems to lead to anomalous behavior, perhaps in part due to larger fluctuations from sampling few sites, but possibly also due to special behavior at the inner most rings.

Inspection of Fig. 6 focusing on behavior for $k_{CC} = 6-10$ furthermore suggests that a discontinuous transition for the model on an infinite Bethe lattice would occur around $p_c \approx 0.05$–0.06. For BC_{Pc}, results for C versus p display a near-vertical line expected for a discontinuous transition around this p range for $k_{CC} = 8-10$. Even results for BC_{MF} are trending toward this behavior. Generally, discontinuous transitions in these models occur slightly below the corresponding spinodal point p_s [6,8]. As for regular Euclidean lattices, the MF site approximation estimate of the spinodal point of $p_s(\text{site}) = \frac{1}{4} = 0.25$ is far too high. However, the pair approximation estimate of $p_s(\text{pair}) = 1/12 \approx 0.0833$ is more reasonable.

Finally, we present some results from conventional constant-p simulation where particle annihilation and creation events are implemented with probabilities proportional to their rates. These simulations enable assessment of time evolution, and specifically the development of heterogeneous steady states. First, we present results in Fig. 7 for BC_{MF} starting with a completely occupied lattice. Figure 7(a) shows that choosing $p = 0.090$ just inside the regime of bistability based on the CC ensemble analysis, ring concentrations C_k initially decrease, but then stabilize to values for a heterogeneous steady state with inner rings having lower concentrations. Similar behavior occurs for lower p also in the regime of bistability, as shown in Appendix C and the SM [21].

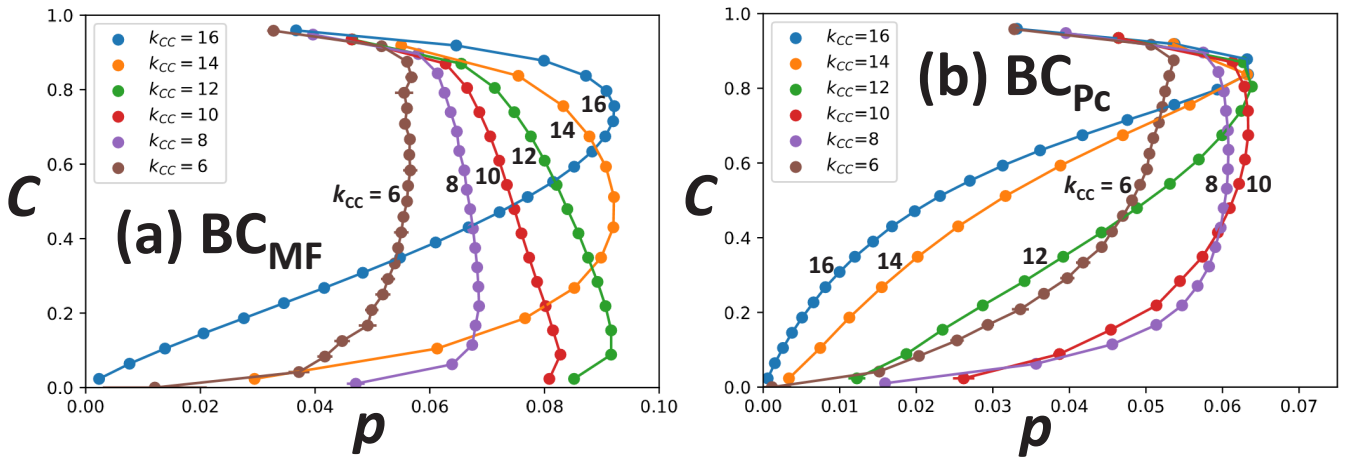

FIG. 6. Results from refined CC simulation where the concentration is just obtained by averaging over ring R_k with $k = k_{CC}$. Behavior for (a) BC_{MF}, (b) BC_{Pc}. Each data point is obtained as an average over 10^4 Monte Carlo steps (MCSs).

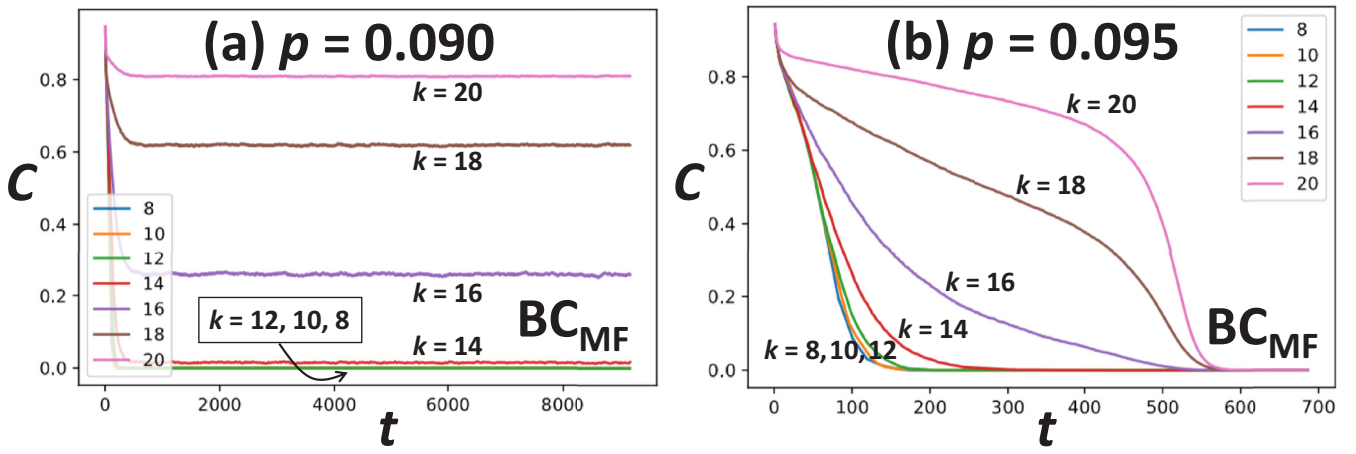

FIG. 7. Evolution of ring concentrations C_k with time t (in MCS) starting with a completely occupied Bethe lattice with $k^* = 20$ for MF BCs. The ring index k is shown in the legend. (a) $p = 0.090$, (b) $p = 0.095$.

Figure 7(b) shows that, choosing $p = 0.095$ presumably just above the regime of bistability, ring concentrations C_k ultimately all decrease to zero, so the system evolves to the vacuum state.

Next, we present results in Fig. 8 for correlated BC_{Pc} again starting with a completely occupied lattice. Figure 8(a) shows that choosing $p = 0.053$ presumably in the regime of bistability, ring concentrations C_k again initially decrease and then stabilize, where now outer rings have lower concentrations. Figure 8(b) shows that choosing higher $p = 0.054$ which from the CC ensemble analysis could plausibly be just above the region of bistability or the discontinuous transition, one finds an initial stabilization of ring concentrations, but then a decrease to zero over longer times as the system evolves to the vacuum state. Similar behavior also occurs for higher p as shown in Appendix C and the SM [21].

Again, our results for BC_{Pc} are expected to best mimic an infinite lattice. Behavior for $p = 0.054$ would be typical for a p value just above the discontinuous transition in an infinite system. Here, the system initially evolves to a metastable populated state, and then more slowly to the stable vacuum steady state. (Such behavior could also reflect noise-induced transitions from a less stable to a more stable steady state in a finite system with bistability, although such transitions tend to occur more suddenly at "random" times.) Thus, these simulations suggest a discontinuous transition between $p = 0.053$ and $p = 0.054$. This result is reasonably consistent with our interpretation of refined CC ensemble simulations. In addition, we cannot rule out the presence of a small p window of generic two-phase coexistence which would lead to slightly different estimates of p_c depending on the simulation protocol [6,9].

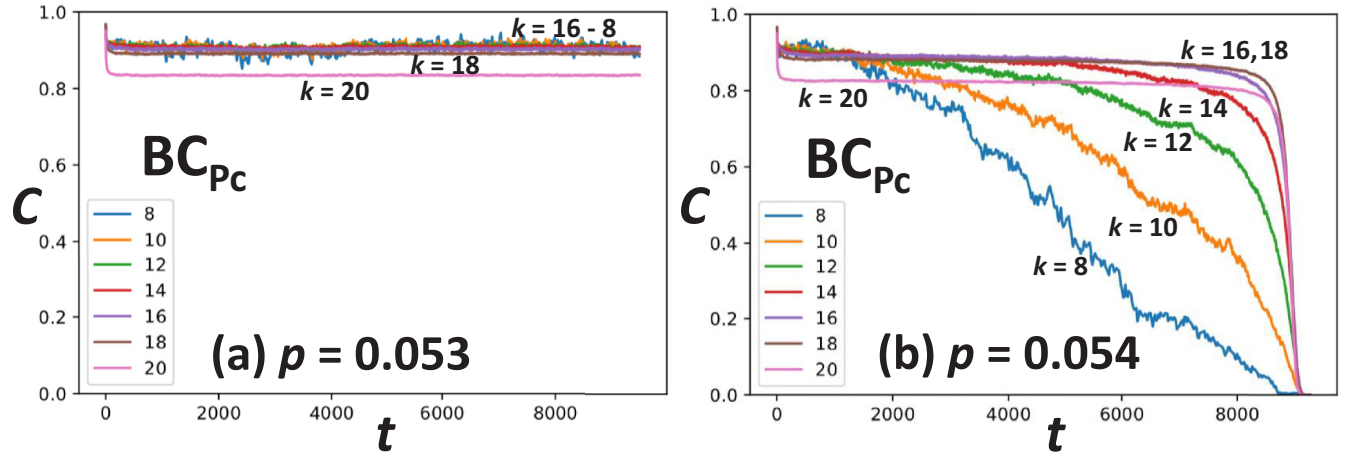

FIG. 8. Time evolution of ring concentrations C_k starting with a completely occupied Bethe lattice with $k^* = 20$ for correlated boundary conditions BC_{Pc}. The ring index k is shown in the legend. (a) $p = 0.053$, (b) $p = 0.054$.

VI. ANALYTIC MF-TYPE ANALYSIS AND INTERPRETATION

For stochastic lattice-gas models with discontinuous phase transitions, mean-field and higher-level hierarchical truncation approximations characterizing homogeneous steady states generally predict a regime of bistability for varying some control parameter p (the particle annihilation rate in our model). Assessment of the location of the discontinuous transition requires consideration of heterogeneous states via lattice differential equations or dRDEs as discussed in Sec. II. For regular Euclidean lattices, one explores the propagation of planar interfaces separating coexisting stable states as a function of p, stationarity of this interface at $p = p_c$ corresponding to the discontinuous transition in the stochastic model. (There can be complications due to pinning or propagation failure and an orientation dependence of p_c which we do not discuss further here [22,36,37].)

For the infinite Bethe lattice in the bistable regime $p \leqslant p_s$, instead of planar interfaces, one can consider the evolution of a droplet of one stable steady state with circular symmetry centered on the origin R_0 (site $j = 1$) embedded in a background of the other steady state. At the mean-field site approximation level, evolution is described by Eqs. (6) and (7). The corresponding more complex equations at the level of the pair approximation were also discussed in Sec. II and are presented in Appendix A. For a populated droplet embedded in the vacuum steady state, it is clear that the droplet cannot propagate outward filling empty sites as those sites have at most one filled neighbor. Such droplets eventually shrink. However, for a vacuum droplet embedded in the populated steady state, in principle such droplets can either shrink or grow. We focus on this latter case below. Specifically, one might anticipate that the vacuum droplet would expand for large p, shrink for small p, and be stationary for a unique value of $p = p_c < p_s$, where p_c plausibly corresponds to the location of the discontinuous transition.

Note that there is an asymmetry in the dRDE due to the Bethe lattice structure, so that propagation of the vacuum droplet outward is distinct from inward propagation. This type of feature was noted in an earlier mean-field study of bistable model dynamics on Bethe lattices [38], although in that study the dRDE had conventional spatial coupling via a discrete Laplacian in contrast to (6).

Numerical analysis using the MF site approximation equations (6) for the case $z = 3$ reveals that an (arbitrarily large) vacuum droplet embedded in the populated state will shrink for $p < 0.243\,503\,4(1)$ and grow for $0.243\,504\,8(6) < p < 0.25$, thus exhibiting a narrow regime of propagation failure of width $\Delta p \approx 0.000\,001\,5$ (also seen for Schloegl's second model on Euclidean lattices [22,23]). The droplet propagation velocity versus p is shown in Appendix D. This suggests a site-approximation estimate of the location of the discontinuous transition as $p_c \approx 0.2435$. However, as indicated above, site-approximation estimates for both spinodals and phase transition points are expected to be far too high, as on Euclidean lattices [22,23].

As an aside, we note that a MF analysis for $z > 3$ reveals that the vacuum droplet shrinks for all p, i.e., for all $0 \leqslant p \leqslant p_s$. See the SM [21]. One might regard the lack of expansion as due to an effective curvature of droplets on the Bethe lattice which is more pronounced for larger z, and which persists for arbitrarily large droplet size. Here, we note that generally curvature inhibits expansion [33–35,39]. Another perspective comes from inspection of (6) which reveals stronger coupling to outer rings for larger z. Thus, e.g., for a vacuum droplet with a sharp interface, the concentration of the initially empty site adjacent to the interface initially grows faster with bigger z. For $z \to \infty$, inspection of (6) shows trivially that the vacuum droplet must shrink. Thus, while large z recovers MF kinetics, front propagation in that regime is nontrivial (as for Euclidean lattices [23]).

Numerical analysis of the pair approximation for $z = 3$ actually reveals that an (arbitrarily large) vacuum droplet shrinks for all $0 \leqslant p \leqslant p_s = 1/12$, suggesting a discontinuous transition at $p_c = p_s = 1/12 \approx 0.0833$. Analogous behavior is also found for $z > 3$. See the SM [21]. Thus, the pair approximation is not as effective as on Euclidean lattices where it correctly indicates a discontinuous transition strictly below the spinodal [8,22,23].

VII. CONCLUSIONS

Our analysis reveals the presence of a discontinuous transition for Schloegl's second model on an infinite Bethe lattice with $z = 3$ occurring at around $p \approx 0.053$. As might be expected, our correlated choice of boundary conditions, BC_{Pa}, BC_{Pb}, or BC_{Pc}, for the finite lattice which accounts for strong spatial correlations in the model can best mimic behavior for infinite lattice. Also our refined CC ensemble simulations are plausibly most effective in extracting infinite lattice behavior from finite lattice simulations. While we have not explicitly performed simulation analysis for cases with $z > 3$, we expect a discontinuous transition also for these cases. Generally, behavior for bigger z reflects more closely the mean-field prediction of bistability, but the presence of noise in the stochastic model ensures the presence of a discontinuous transition. This view is consistent with the results in Ref. [17] which considers a discrete-time version of Schloegl's second model.

ACKNOWLEDGMENTS

D.-J.L. and J.W.E. were supported by the USDOE BES Division of Chemical Sciences, Geosciences, and Biosciences through the Chemical Physics project at Ames Laboratory. Ames Laboratory is operated by Iowa State University under Contract No. DE-AC02-07CH11358. C.-J.W. was supported by the Ministry of Science and Technology (MOST) of Taiwan, Grant No. 109-2115-M-194-004-MY2.

APPENDIX A: SPATIALLY HETEROGENEOUS FACTORIZATION APPROXIMATIONS

In the mean-field site approximation, the coupled lattice differential equations describing the evolution of ring concentrations, $P_{\bullet_k} = C_k$, were presented in Sec. III as Eqs. (6) and (7).

In the pair approximation, we obtain a coupled set of equations for $P_{\bullet_k} = C_k$ and $P_{o_{k-1}o_k} = D_{k-1,k}$. As noted in Sec. III, one writes $P_{\bullet_{k-1}o_k\bullet_{k+1}} \approx P_{\bullet_{k-1}o_k} P_{o_k\bullet_{k+1}}/P_{o_k}$,

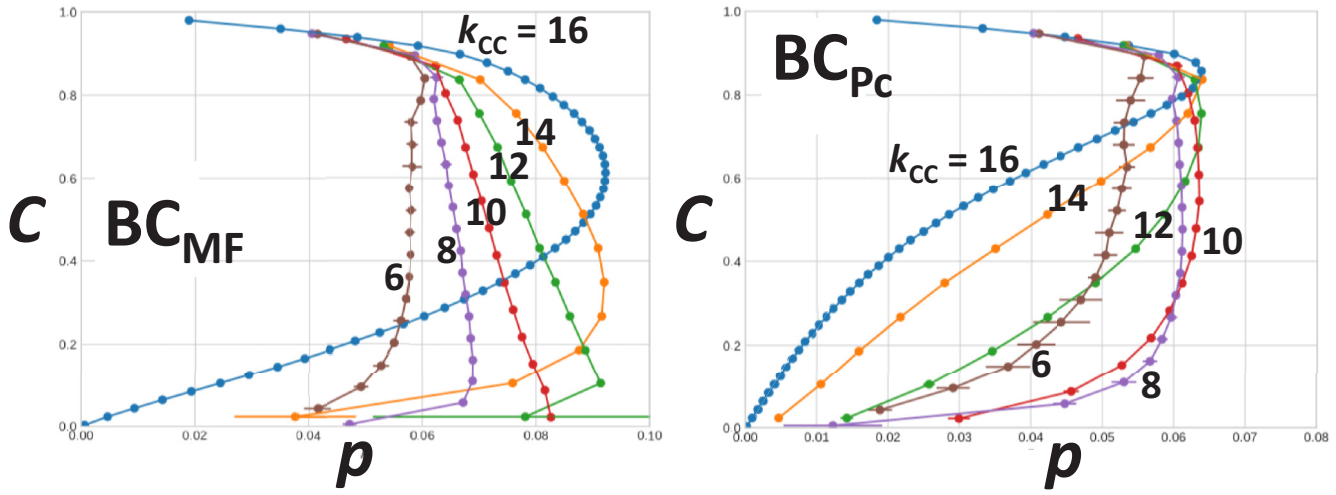

FIG. 9. Results from refined CC simulation with concentration obtained by averaging over rings R_k with $k = 1$ through k_{CC}. Behavior for BC_{MF} (BC_{Pc}) is shown on the left (right).

etc. Applying this factorization to the equations in Fig. 2 yields

$$d/dtP\bullet_k = -pP\bullet_k + z^{-1}\left[2P\bullet_{k-1}o_kPo_k\bullet_{k+1} + (z-2)(Po_k\bullet_{k+1})^2\right]/Po_k \quad \text{for } k \geqslant 1, \tag{A1}$$

$$\begin{aligned} d/dtPo_{k-1}o_k = {} & +pP\bullet_{k-1}o_k + pPo_{k-1}\bullet_k \\ & - (z-2)z^{-1}(z-1)^{-1}\left[2P\bullet_{k-2}o_{k-1}Po_{k-1}\bullet_k + (z-3)(Po_{k-1}\bullet_k)^2\right]Po_{k-1}o_k/(Po_{k-1})^2 \\ & - (z-2)z^{-1}(Po_k\bullet_{k+1})^2Po_{k-1}o_k/(Po_k)^2, \quad \text{for } k \geqslant 2, \end{aligned} \tag{A2}$$

with separate relations for $k = 0$ and 1. Using conservation of probability relations such as $P\bullet_{k-1}o_k + Po_{k-1}o_k = Po_k$, and $Po_{k-1}\bullet_k + Po_{k-1}o_k = Po_{k-1}$, then (A1) and (A2) become

$$d/dtC_k = -pC_k + \left[2(1-C_k-D_{k-1,k})(1-C_k-D_{k,k+1}) + (z-2)(1-C_k-D_{k,k+1})^2\right]/(1-C_k) \quad \text{for} \quad k \geqslant 1, \tag{A3}$$

$$\begin{aligned} d/dtD_{k-1,k} = {} & +p(1-C_k-D_{k-1,k}) + p(1-C_{k-1}-D_{k-1,k}) - (z-2)z^{-1}(z-1)^{-1}[2(1-C_{k-1}-D_{k-2,k-1}) \\ & \times (1-C_{k-1}-D_{k-1,k}) + (z-3)(1-C_{k-1}-D_{k-1,k})^2]D_{k-1,k}/(1-C_{k-1})^2 - (z-2)z^{-1} \\ & \times (1-C_k-D_{k,k+1})^2D_{k-1,k}/(1-C_{k-1})^2, \quad \text{for } k \geqslant 2, \end{aligned} \tag{A4}$$

with separate relations for $k = 0$ and 1.

APPENDIX B: REFINED CC SIMULATION ANALYSIS

Figure 9 shows the results for $z = 3$ from implementing a refined CC simulation ensemble procedure where the concentration is rings R_k with $k = 1$ through k_{CC} are sampled and compared with the target concentration. Thus, the choice $k_{CC} = k^*$ sampling over the entire system just corresponds to the standard CC ensemble. Behavior is compared for the BC_{MF} and BC_{Pc} boundary conditions. Similar results are obtained in Fig. 6 just sampling a single ring with $k = k_{CC}$. Again, similar features emerge for the different BCs when selecting $k_{CC} = 8-10$ for $k^* = 16$. Also, again these results are suggestive of a discontinuous transition in Schloegl's second model on an infinite Bethe lattice around $p_c \approx 0.055$–0.06.

APPENDIX C: CONSTANT-p SIMULATIONS OF TIME EVOLUTION

We present additional results from conventional constant-p simulations for time evolution starting from an initially fully populated state. Figure 10 shows results for BC_{MF}, and Fig. 11 shows results for BC_{Pc} for a range of p.

Some additional comments are appropriate for MF BC. For $p \leqslant 0.05$, the steady state is almost homogeneous. For $0.06 \leqslant p \leqslant 0.09$, the steady state becomes strongly heterogeneous with outer rings heavily populated and inner rings almost empty. This is somewhat reminiscent of coexistence of populated and vacuum states separated by an interface, and the feature that it occurs over a range of p is somewhat reminiscent of generic two-phase coexistence. For $p \geqslant 0.095$, the system evolves to the vacuum state. See Fig. 7 and the SM.

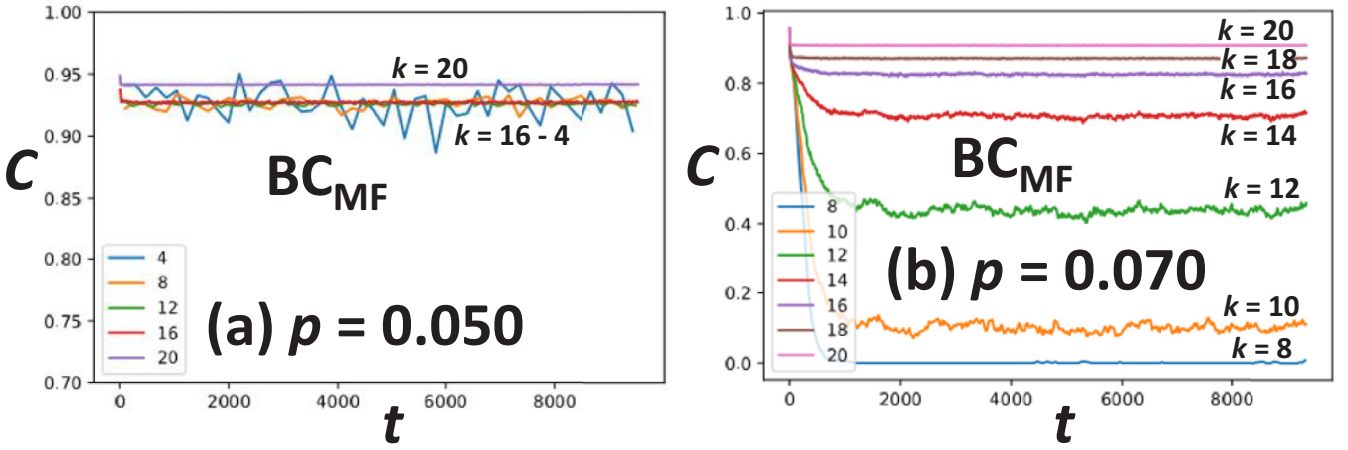

FIG. 10. Evolution of concentrations C_k for various rings, k (labeled in the legend) for BC_{MF} boundary conditions for: (a) $p = 0.050$; (b) $p = 0.070$, with a populated heterogeneous steady state.

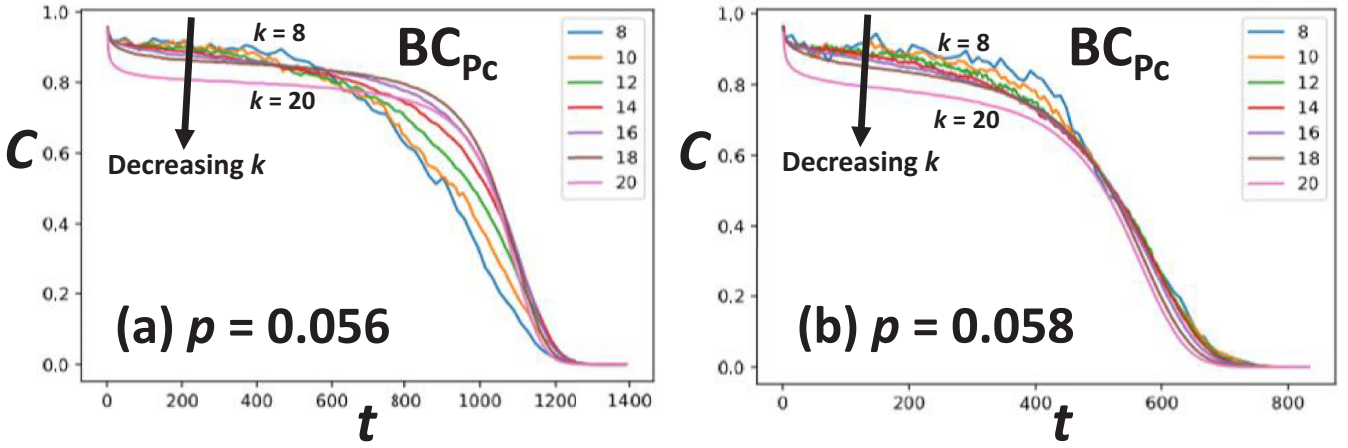

FIG. 11. Evolution of concentrations C_k for various rings k (labeled in the legend) with BC_{Pc} for: (a) $p = 0.056$; (b) $p = 0.058$, above the discontinuous transition showing evolution to the vacuum state.

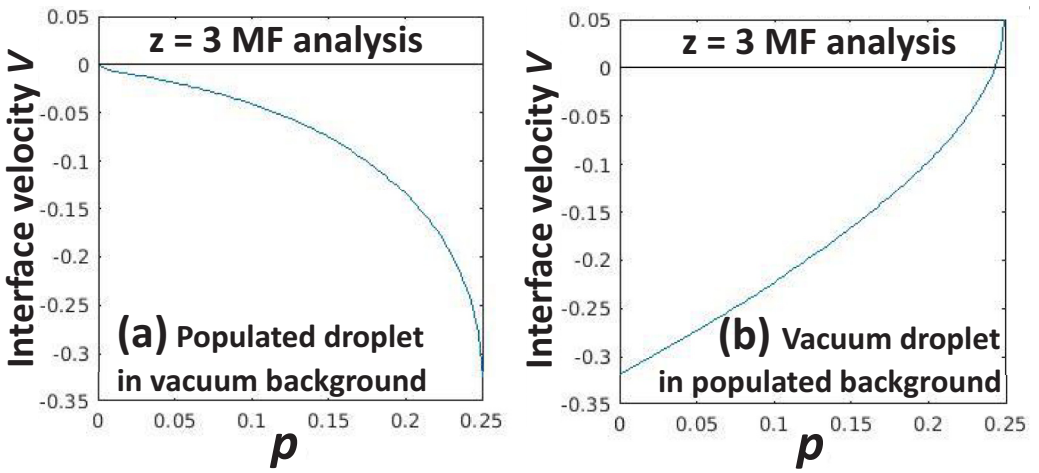

FIG. 12. MF estimate of the propagation velocity V versus p of a large droplet of (a) the populated steady state embedded in the vacuum state, (b) the vacuum state embedded in the populated steady state.

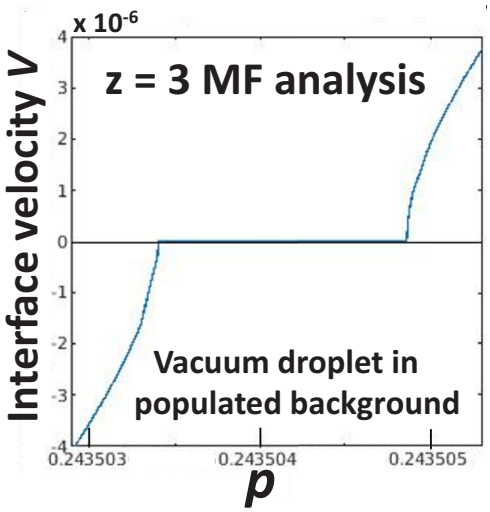

FIG. 13. MF estimate of the propagation velocity V versus p of a large droplet of the vacuum state embedded in the populated steady state near the propagation failure region. This plot corresponds to a zoomed-in version of Fig. 12(b) around $p = 0.243\,504$.

APPENDIX D: DROPLET EVOLUTION IN ANALYTIC TRUNCATION APPROXIMATIONS

Using the MF equations (6) and (7) describing interface propagation for states with circular symmetry, we analyze the propagation of a very large droplet of one stable phase centered on site $j = 1$ embedded in the other phase. We define the propagation velocity V of the droplet interface as positive ($V > 0$) if the droplet grows, and negative ($V < 0$) in the opposite case. Figure 12 shows the results from a MF analysis for $z = 3$. Figure 12(a) shows that the populated droplet always shrinks, a trivial consequence of the model prescription. Figure 12(b) shows that the vacuum droplet shrinks except for a small range of p such that roughly $0.243\,50 < p \leqslant 0.25$. Closer inspection of behavior around the apparent equistability point, $p_c \approx 0.243\,50$, actually reveals a narrow regime of propagation failure for $0.243\,503\,4(1) < p < 0.243\,504\,8(6)$, as noted in the text. See Fig. 13. Also, as noted in the text, the pair approximation predicts droplet shrinkage in all cases, i.e., there is no equistability point or propagation failure in the case of a vacuum droplet.

[1] J. Marro and R. Dickman, *Nonequilibrium Phase Transitions in Lattice Models* (Cambridge University Press, Cambridge, UK, 1999).
[2] G. Odor, Rev. Mod. Phys. **76**, 663 (2004).
[3] M. Henkel, H. Hinrichsen, and S. Luebeck, *Non-Equilibrium Phase Transitions* (Springer, Berlin, 2008), Vol. 1.
[4] F. Schloegl, Z. Phys. **253**, 147 (1972).
[5] R. Durrett, SIAM Rev. **41**, 677 (1999).
[6] D.-J. Liu, X. Guo, and J. W. Evans, Phys. Rev. Lett. **98**, 050601 (2007).
[7] S. Handjani, J. Theor. Probab. **10**, 737 (1997).
[8] C.-J. Wang, D.-J. Liu, and J. W. Evans, J. Chem. Phys. **142**, 164105 (2015).
[9] D.-J. Liu, C.-J. Wang, and J. W. Evans, Phys. Rev. Lett. **121**, 120603 (2018).
[10] H. A. Bethe, Proc. Roy. Soc. London, Ser. A **150**, 552 (1935).
[11] M. Ostilli, Phys. A (Amsterdam, Neth.) **391**, 3417 (2012).
[12] R. J. Baxter, *Exactly Solved Models in Statistical Mechanics* (Academic, London, 1982).
[13] D. Stauffer and A. Aharony, *Introduction to Percolation Theory*, Revised 2nd ed. (CRC, Boca Raton, 2000).
[14] J. W. Evans, J. Phys. A **20**, 6487 (1987).
[15] S. N. Dorogovtsev, A. V. Goltsev, and J. F. F. Mendes, Rev. Mod. Phys. **80**, 1275 (2008).
[16] L. R. G. Fontes and R. H. Schonmann, Probab. Theory Relat. Fields **141**, 513 (2008).
[17] S. Chatterjee and R. Durrett, Stoch. Proc. Appl. **123**, 561 (2013).
[18] C. Varghese and R. Durrett, Phys. Rev. E **87**, 062819 (2013).
[19] W. Li, J. von Delft, and T. Xiang, Phys. Rev. B **86**, 195137 (2012).
[20] Y. Lee, F. Verstraete, and A. Gendiar, Phys. Rev. E **94**, 022133 (2016).
[21] See Supplemental Material at http://link.aps.org/supplemental/10.1103/PhysRevE.104.014135 for (SM1) description of site labeling on the Bethe lattice for $z = 3$; (SM2) constant-p simulations for time evolution; and (SM3) mean-field analysis of dRDE for the velocity of propagation of droplets.
[22] X. Guo, J. W. Evans, and D.-J. Liu, Physica (Amsterdam) A **387**, 177 (2008).
[23] C.-J. Wang, D.-J. Liu, and J. W. Evans, Phys. Rev. E **85**, 041109 (2012).
[24] J. W. Evans, Langmuir **7**, 2514 (1991).
[25] J. W. Evans, Rev. Mod. Phys. **65**, 1281 (1993).
[26] R. M. Ziff and B. J. Brosilow, Phys. Rev. A **46**, 4630 (1992).
[27] T. Tome and M. J. de Oliveira, Phys. Rev. Lett. **86**, 5643 (2001).
[28] J. W. Evans, D.-J. Liu, and M. Tammaro, Chaos **12**, 131 (2002).
[29] M. Tammaro, M. Sabella, and J. W. Evans, J. Chem. Phys. **103**, 10277 (1995).
[30] Yu. Suchorski, J. Beben, E. W. James, J. W. Evans, and R. Imbihl, Phys. Rev. Lett. **82**, 1907 (1999).
[31] Yu. Suchorski, J. Beben, R. Imbihl, E. W. James, D.-J. Liu, and J. W. Evans, Phys. Rev. B **63**, 165417 (2001).
[32] D.-J. Liu and J. W. Evans, J. Chem. Phys. **117**, 7319 (2002).
[33] A. S. Mikhailov, *Foundations of Synergetics I* (Springer, Berlin, 1994).
[34] X. Guo, D.-J. Liu, and J. W. Evans, J. Chem. Phys. **130**, 074106 (2009).
[35] D.-J. Liu and J. W. Evans, Prog. Surf. Sci. **88**, 393 (2013).
[36] S.-N. Chow, J. Mattel-Paret, and E. S. van Vleck, Int. J. Bifurcation Chaos **06**, 1605 (1996).
[37] G. Fath, Phys. D (Amsterdam, Neth.) **116**, 176 (1998).
[38] N. E. Kouvaris, H. Kori, and A. S. Mikhailov, PLoS One **7**, e45029 (2012).
[39] C.-J. Wang, D.-J. Liu, and J. W. Evans, Phys. Rev. E **101**, 022803 (2020).